Important Influence of North Atlantic Oscillation on Interannual Variability of the Boreal Autumn East Siberian–Beaufort Sea Ice

LI LIU,[a] WENJUN ZHANG,[a] CHAO LIU,[a,b] AND FENG JIANG[a]

[a] *CIC-FEMD/ILCEC, Key Laboratory of Meteorological Disaster of Ministry of Education (KLME), Nanjing University of Information Science and Technology, Nanjing, China*
[b] *Irreversible Climate Change Research Center, Yonsei University, Seoul, South Korea*

(Manuscript received 7 June 2023, in final form 28 October 2023, accepted 4 November 2023)

ABSTRACT: The East Siberia–Beaufort Sea (EsCB) sea ice during boreal autumn has recently been reported to play important roles in the climate over Eurasia and North America. The EsCB sea ice exhibits remarkable year-to-year fluctuations in autumn (August–October), the season in which its minimum extent usually occurs. However, the physical driver of the autumn EsCB sea ice interannual variability remains unclear, impeding the seasonal prediction of local sea ice. Here we find that the autumn EsCB sea ice variability is largely driven by the preceding summer (May–July) dipolar atmospheric anomalies over the North Atlantic, resembling the North Atlantic Oscillation (NAO) pattern. During the negative NAO-like phase, the circumpolar anticyclonic anomalies tend to transport the warm air from Greenland toward the EsCB region, which triggers rapid sea ice melt there. The associated EsCB sea ice anomalies can be maintained or even intensified by the local sea ice–albedo positive feedback until autumn. Therefore, the abnormal signals of Arctic sea ice tend to show significant persistence in summer and autumn. The influence of the summer NAO-like atmospheric circulation on the ensuing autumn EsCB sea ice can be realistically reproduced in the historical simulation of the E3SM-1-0 model, supporting our findings based on the observation. This lagged relationship provides a promising pathway for skillful seasonal prediction of the EsCB sea ice and its related climatic impacts.

KEYWORDS: Sea ice; Interannual variability; North Atlantic Oscillation

1. Introduction

As a major element of Earth's climate system, Arctic sea ice has been receiving scientific and public attention since it is a key indicator of global climate change due to its sensitivity to anthropogenic warming (Barry et al. 1993; Stroeve et al. 2007; Cavalieri and Parkinson 2012; Parkinson 2014). Sea ice typically covers the entire Arctic Ocean in the boreal winter season, melts during the summer season, and reaches a minimum around September (Parkinson and Cavalieri 1989; Serreze et al. 2007; Eisenman 2010; Stroeve and Notz 2018; Bliss et al. 2019). Arctic sea ice can influence the local climate through the heat exchange between the ice-covered ocean and its above atmosphere (Aagaard and Carmack 1989; Curry et al. 1995; Serreze et al. 2007; Vihma 2014; Gao et al. 2015; Lei et al. 2016). It can also affect the remote climate in the mid-to-high latitudes of the Northern Hemisphere or even at the global scale via atmospheric teleconnections (e.g., Wallace and Gutzler 1981; Budikova 2009; Honda et al. 2009). Understanding the mechanisms responsible for the Arctic sea ice change is thus critical for better predictions of the Arctic climate and associated ecological environment.

Over the past several decades, the Arctic sea ice amount experienced a rapid decline (e.g., Rothrock et al. 1999; Comiso et al. 2008; Kwok and Rothrock 2009; Parkinson 2014). For example, in September 2007, the Arctic sea ice extent reached a record minimum since the satellite observation, and this record was later refreshed in 2012. It is generally believed that the continuous sea ice loss is mainly contributed by the anthropogenic forcing and is further worsened due to local positive feedback (e.g., the sea ice–albedo feedback and the cloud–radiative feedback) (Gillett et al. 2008; Ding et al. 2017; Baxter et al. 2019). Superimposed on the long-term decline, the sea ice also exhibits a remarkable interannual variability, which is suggested to be linked with many internal climate modes, such as El Niño–Southern Oscillation (ENSO) and the North Atlantic Oscillation (NAO) (Wang et al. 1994; Hu et al. 2016; Ukita et al. 2016). When a central-Pacific (CP) El Niño event occurs, the tropospheric Arctic polar vortex and the circumpolar westerly wind are enhanced due to the stationary atmospheric Rossby waves associated with the tropical Pacific convection, suppressing the summer Arctic warming and the sea ice melting (Hu et al. 2016). In addition, the strong and westward displaced NAO event in winter favors negative surface air temperature anomalies over the Baffin Bay–Labrador region, leading to positive anomalies of the local sea ice in the simultaneous winter and the subsequent spring (Wang et al. 1994). Besides, the drastic atmospheric circulation anomalies, such as the strong Arctic dipole anomaly and an intense local cyclone, can drive the extremely low sea ice events via local atmospheric heating, wind-induced sea ice drift, and the cloud–radiative feedback (e.g., Ogi and Wallace 2007; Stroeve et al. 2008; Wang et al. 2009; Nussbaumer and Pinker 2012; Wu et al. 2012; Zhang et al. 2013; Cui et al. 2015; Kirchmeier-Young et al. 2017).

Earlier studies often treated the Arctic sea ice as a whole and its spatial inhomogeneity was less considered, which could cause an ambiguous understanding of the local sea ice variability (Screen et al. 2014; Close et al. 2015). Many recent

Corresponding author: Wenjun Zhang, zhangwj@nuist.edu.cn

DOI: 10.1175/JCLI-D-23-0341.1

© 2023 American Meteorological Society. This published article is licensed under the terms of the default AMS reuse license. For information regarding reuse of this content and general copyright information, consult the AMS Copyright Policy (www.ametsoc.org/PUBSReuseLicenses).

Unauthenticated | Downloaded 11/13/26 12:37 PM UTC

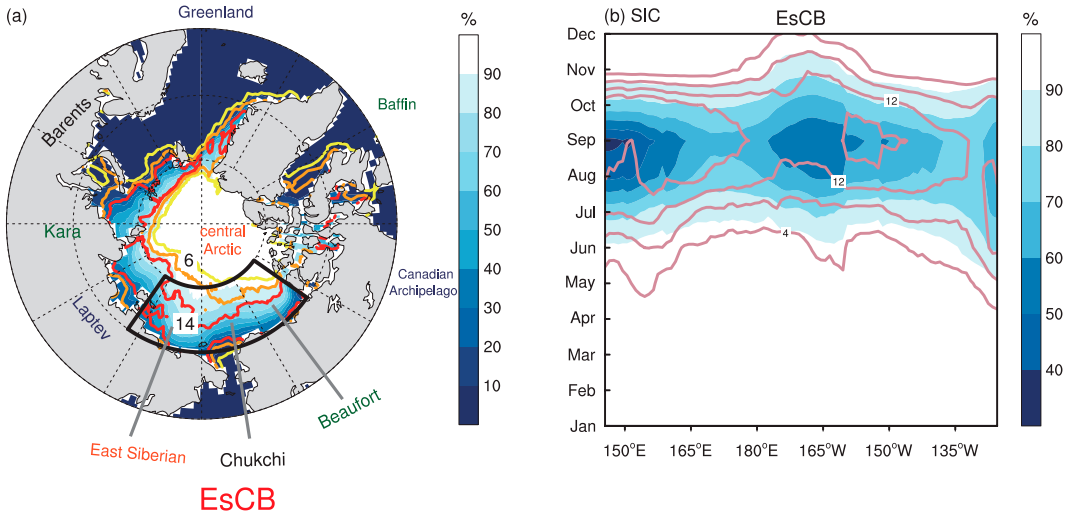


FIG. 1. (a) Climatological mean (shading; %) and interannual standard deviation (contours; %) of August–October (ASO) Arctic sea ice. The interannual standard deviation increases as the color transitions from yellow to red, indicating the larger variations. The black sector indicates the EsCB region (70°–80°N, 145°E–125°W). (b) Time–longitude evolution of meridional (70°–80°N) averaged sea ice seasonal cycle (shading; %) and its interannual standard deviation (contours; %).

studies divided the Arctic sea ice into subdomains to explore their regional climate impacts (e.g., Meier et al. 2007; Bliss et al. 2019; Nie et al. 2022; Onarheim et al. 2018; Peng and Meier 2017; Zuo et al. 2016). In particular, the sea ice over the Barents–Kara (BK) Seas has received much attention considering that it is one of the main sources of cold air in Eurasian winter (Francis et al. 2009; Petoukhov and Semenov 2010; Wu et al. 2011; Chen et al. 2014; Chen and Wu 2018; Mori et al. 2014, 2019). It is suggested that the interannual variability of the BK sea ice could be explained by the local sea ice conditions (e.g., ice age or thickness; Spreen et al. 2011; Carmack et al. 2015), the inflow of Atlantic warm water (Schlichtholz 2011; Herbaut et al. 2015), advection of sea ice from other Arctic regions (Wu et al. 2006; Wu and Johnson 2007; Lind et al. 2018), and the variation of local wind anomalies (Pavlova et al. 2014). Aside from the BK sea ice, the East Siberian–Beaufort (EsCB) sea ice has received increasing attention in recent years, since the decreasing trend of EsCB sea ice is the strongest in the Arctic region during the boreal autumn season (Comiso 2002; Onarheim et al. 2018; Peng and Meier 2017; Liu et al. 2021; Kug et al. 2015; Chen and Wu 2018; Ding et al. 2021). It has been suggested that the melting of EsCB sea ice is accompanied by the development of a local anomalous anticyclone as well as a downstream midlatitude trough, both of which are conducive to the late cooling of central North America (Kug et al. 2015). A reduction of EsCB sea ice can also favor simultaneous tropospheric warming and positive geopotential height anomalies one month later in the Arctic region. This anticyclonic anomaly further extends southward into west-central Eurasia and leads to surface cooling there (Ding et al. 2021).

At present, the characteristics and physical causes of the EsCB sea ice on the interannual time scale, are still poorly understood. In this study we focus on the characteristics of the autumn EsCB sea ice interannual variability and explore its possible physical driver. In the remainder of this paper, section 2 describes the utilized datasets and methodologies. Section 3 shows the characteristics of the EsCB sea ice interannual variability during the autumn season and its linkage with the NAO-like atmospheric anomalies. In section 4, the associated physical mechanism is explored and further verified based on the E3SM-1-0 historical simulation from phase 6 of the Coupled Model Intercomparison Project (CMIP6). The major conclusions are summarized and discussed in section 5.

2. Data and methodology

The monthly mean sea surface temperature (SST) and sea ice concentration (SIC) are obtained from the Met Office Hadley Centre Sea Ice and Sea Surface Temperature datasets (HadISST) (Rayner et al. 2003). The SIC represents the percentage of sea ice coverage per unit grid. We also use several atmospheric variables from the National Centers for Environmental Prediction–National Center for Atmospheric Research (NCEP–NCAR), including geopotential height, sea level pressure, and surface heat flux (Kalnay et al. 1996). The monthly mean NAO index is provided by the Climate Prediction Center (CPC), based on rotated principal component analysis following Barnston and Livezey (1987). Almost the same results can be derived based on other definitions of the NAO index (e.g., Hurrell 1995; Li and Wang 2003). Monthly outputs (1950–2014) from the historical simulation of E3SM-1-0 climate model that participated in CMIP6 are examined to further validate our observational findings. E3SM-1-0 is a fully coupled Earth system model from the U.S. Department of Energy. The model includes different components of atmosphere and land (110 km grid spacing) and ocean and sea ice (60 km in the

Unauthenticated | Downloaded 11/13/26 12:37 PM UTC

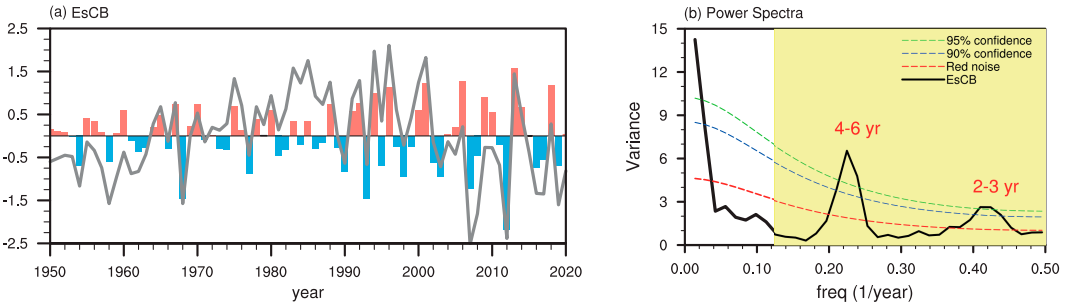


FIG. 2. (a) Time series of the normalized detrended (gray line) and interannual (bars) autumn EsCB index. (b) Power spectra of the normalized ASO EsCB index. The golden shading highlights the interannual (<8 years) time scale. The red dashed line is the red-noise spectrum inferred from a first-order autoregressive process, while blue and green lines represent the associated 90% and 95% confidence intervals.

midlatitudes, 30 km at the equator and poles). This model has been widely applied in studies of Arctic sea ice change and related climate impacts (Petersen et al. 2019; Jeong et al. 2020; Lee et al. 2020). It has the authenticity of the simulated Arctic Ocean and sea ice conditions with refined processes such as sea ice mass and salt exchange (Golaz et al. 2019; Bogenschutz et al. 2020; Veneziani et al. 2022), while most current climate models have a large deficiency (e.g., Notz et al. 2016; Notz and SIMIP Community 2020).

In this study, the interannual sea ice variability in the boreal autumn season [i.e., August–October (ASO)] is our focus, and anomalies were calculated as the departures from the climatological monthly mean for the entire study period (1950–2020). A high-pass Fourier filter with an 8-yr cutoff period is applied to exclude possible impacts from the decadal variability or global warming. It is noted that the qualitative conclusion remains the same using original data or detrended data. The area-averaged SIC over the EsCB (70°–80°N, 145°E–125°W) is defined as the EsCB index for convenience. All the regression coefficients are multiplied by a factor of −1 to illustrate the conditions associated with the reduced SIC or the negative NAO-like atmospheric anomalies. We also perform composite analyses to highlight the differences between high and low sea ice years, which are identified by a threshold of 0.8 standard deviations of the normalized EsCB sea ice index. All statistical significance tests for correlation, regression, and composite analyses are determined based on the two-tailed Student's *t* test. Similar conclusions can be obtained based on the ERA5 dataset (the fifth generation of the ECMWF atmospheric reanalysis of the global climate).

3. Interannual variability of EsCB sea ice and its linkage with the NAO

Figure 1a shows the climatological mean state and standard deviation of the boreal autumn Arctic sea ice. The climatological

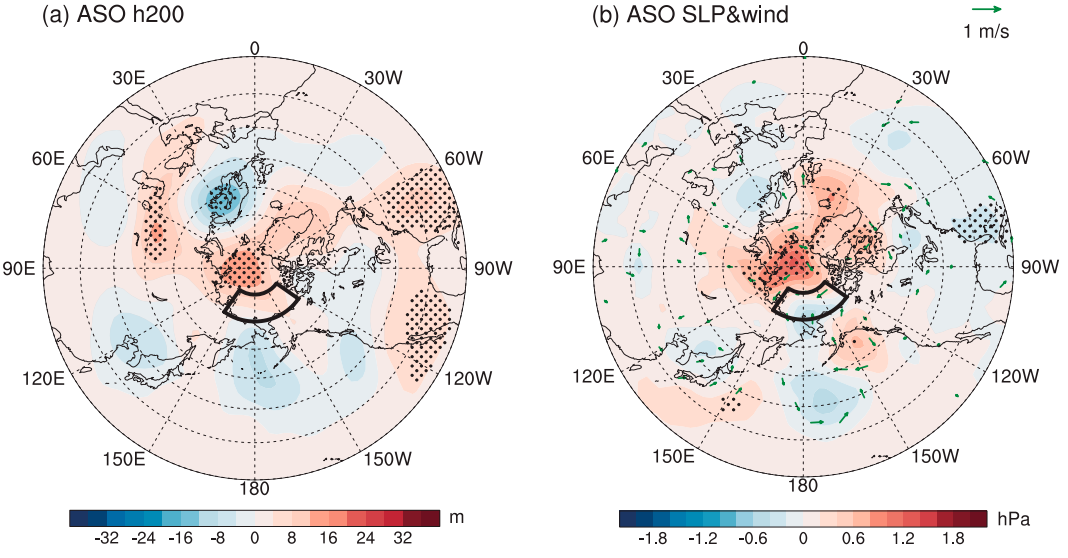


FIG. 3. (a) Regressed 200-hPa geopotential height anomalies (shading; m) in ASO upon the normalized ASO EsCB index. (b) As in (a), but for the sea level pressure (shading; hPa) and surface wind (vectors; m s^{-1}) anomalies. Only values exceeding the 95% confidence level are stippled (shading) or shown (vectors). The black box indicates the EsCB region. The regression coefficients were multiplied by a factor of −1.

Unauthenticated | Downloaded 11/13/26 12:37 PM UTC

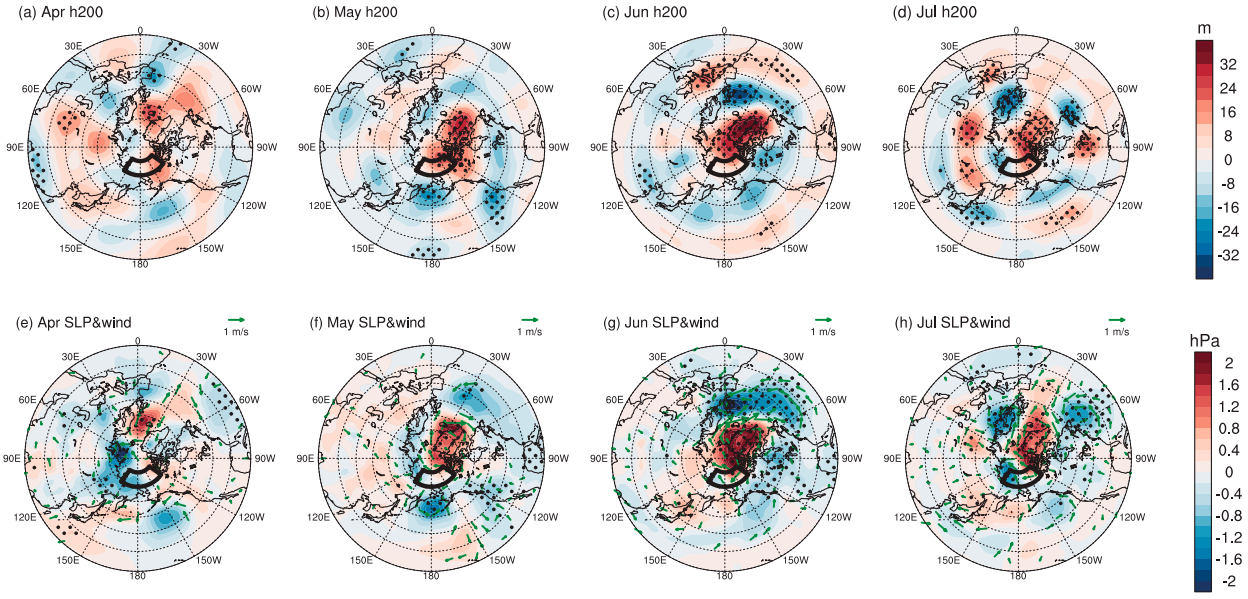


FIG. 4. Regressed 200-hPa geopotential height anomalies (shading; m) upon the normalized ASO EsCB index in (a) April, (b) May, (c) June, and (d) July. (e)–(h) As in (a)–(d), but for the SLP (shading; hPa) and surface wind (vectors; m s^{-1}) anomalies. Only values exceeding the 95% confidence level are stippled (shading) or shown (vectors). The black box indicates the EsCB region. The regression coefficients were multiplied by a factor of −1.

sea ice area where the SIC is larger than 90% is mainly concentrated around the central Arctic. Between the Arctic pole and open waters, there is a noticeable transition zone of ice–water mixing, where the climatological SIC gradually decreases to the south with a large interannual variability (Fig. 1a). The EsCB region exhibits pronounced sea ice melting and significantly larger ice–water mixing compared to other Arctic areas in autumn, establishing the autumn EsCB sea ice as the primary focus for interannual variations in Arctic. For the EsCB region, it consists of the East Siberia Sea, Chukchi Sea, and the Beaufort Sea. During boreal winter and spring, the EsCB region is almost completely covered by sea ice, which starts to melt in late spring (Fig. 1b) and reaches the minimum in autumn (ASO). The SIC interannual variability is weak in winter and spring, while the SIC displays prominent year-to-year fluctuations in summer and autumn. In particular, the largest EsCB SIC interannual variability is observed during autumn (Figs. 1b and 2a). Based on the power spectrum of the EsCB index, there are two significant interannual spectral peaks with dominant periodicities centered around 2–3 and 4–6 years,

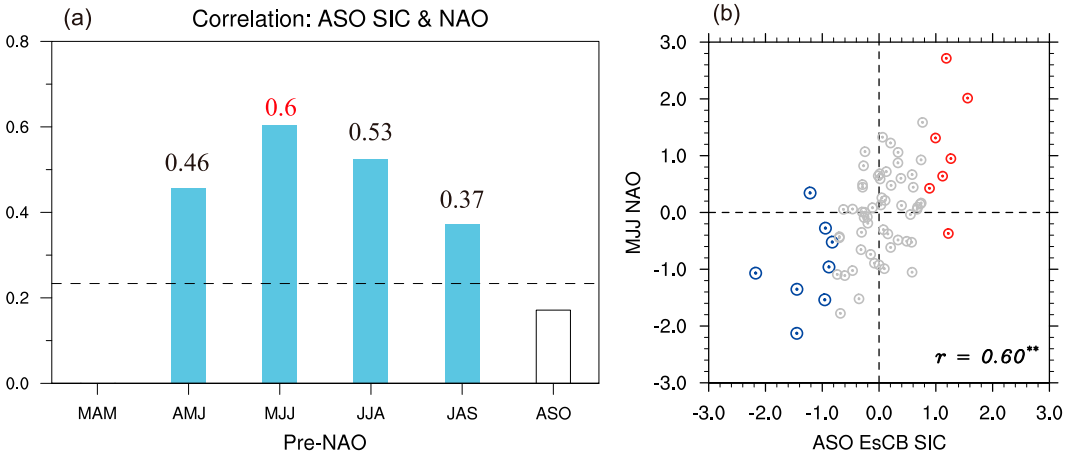


FIG. 5. (a) Correlation coefficients (bar) of the ASO EsCB index with the NAO index in previous seasons. The horizontal dashed line represents the 95% confidence level. (b) Scatterplot of the normalized MJJ NAO index and the EsCB index. Blue, gray, and red circles denote the years with low, normal, and high EsCB SIC in ASO. The correlation coefficient (r) is labeled in the bottom-right corner of the panel.

Unauthenticated | Downloaded 11/13/26 12:37 PM UTC

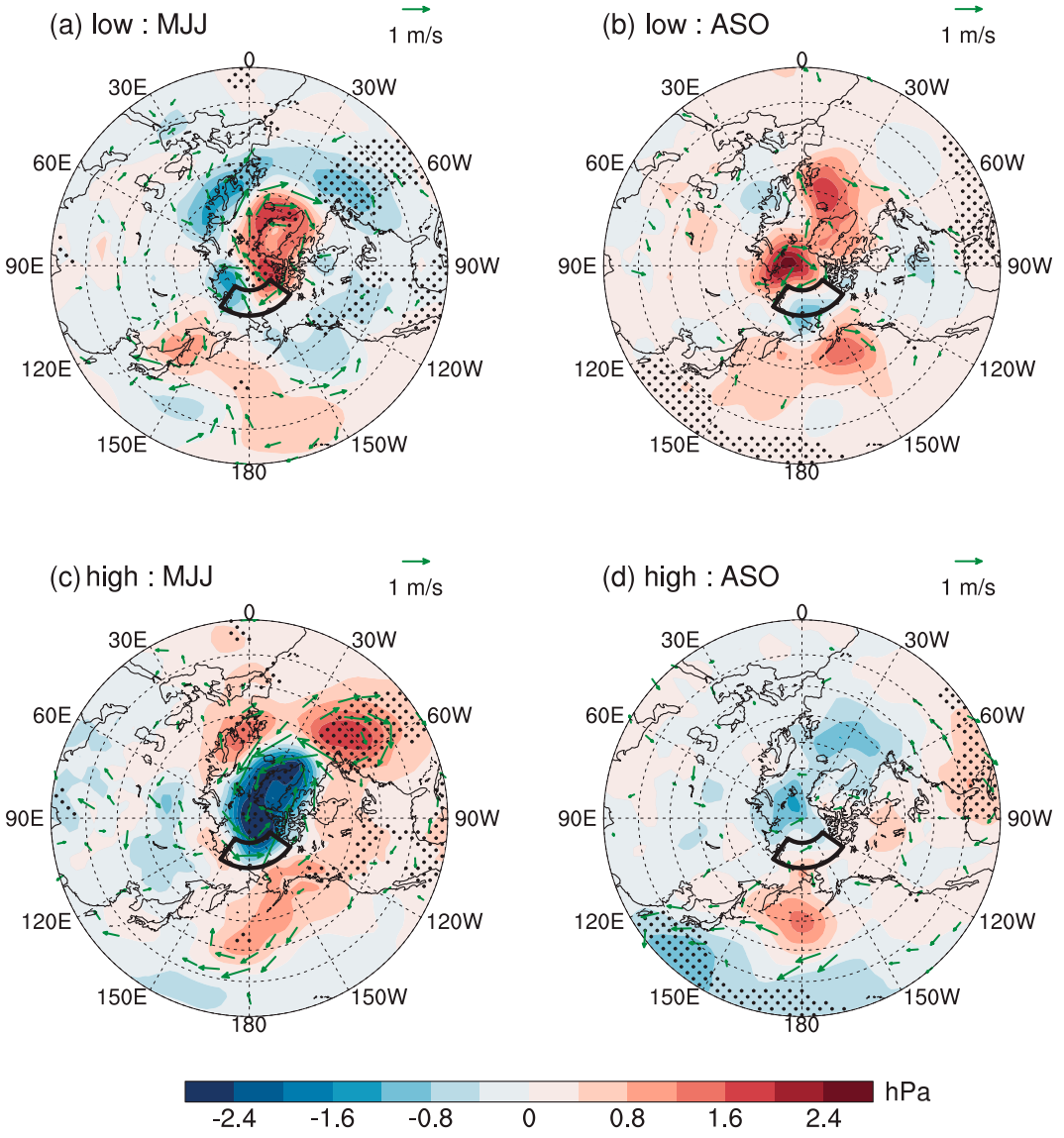


FIG. 6. Composites of SLP anomalies (shading; hPa) and surface wind anomalies (vectors; m s^{-1}) for the low EsCB SIC years in (a) MJJ and (b) ASO. (c),(d) As in (a) and (b), but for the high EsCB SIC years. Only values exceeding the 95% confidence level are stippled (shading) or shown (vectors). The black box indicates the EsCB region.

respectively (Fig. 2b). It is noted that the detrended EsCB index also exhibits multidecadal fluctuations besides the prominent interannual variability (Fig. 2a), which is possibly associated with the Atlantic multidecadal oscillation (Liu et al. 2023). Considering the possible disturbance of the background decadal variability, the high-frequency (8-yr) filtering is conducted to focus on the interannual component of the EsCB sea ice.

To examine possible physical processes associated with the interannual variability of the autumn EsCB sea ice, we first show the simultaneous atmospheric circulations based on the regression analyses (Fig. 3). Anomalously higher geopotential height in association with reduced autumn EsCB sea ice is observed north of the EsCB from the surface to the upper troposphere. Over the EsCB region, the atmospheric anomalies are rather weak, suggesting that the local simultaneous atmospheric forcings could not explain the interannual variations of the EsCB sea ice. As the SIC anomalies could be a response to integrated atmospheric forcings in previous months (e.g., Ogi and Wallace 2007; Wang et al. 2009), we next perform a lagged regression analysis, in which pronounced atmospheric anomalies appear at the lead time of around one season (Fig. 4). Corresponding to the reduction of autumn EsCB SIC, an anomalous anticyclonic circulation is observed on the eastern side of Greenland in April and an anomalous cyclonic circulation over the Barent-Kara Sea (Fig. 4e). Subsequently, the anomalous anticyclone near Greenland is strongly enhanced and shifted toward the EsCB region

Unauthenticated | Downloaded 11/13/26 12:37 PM UTC

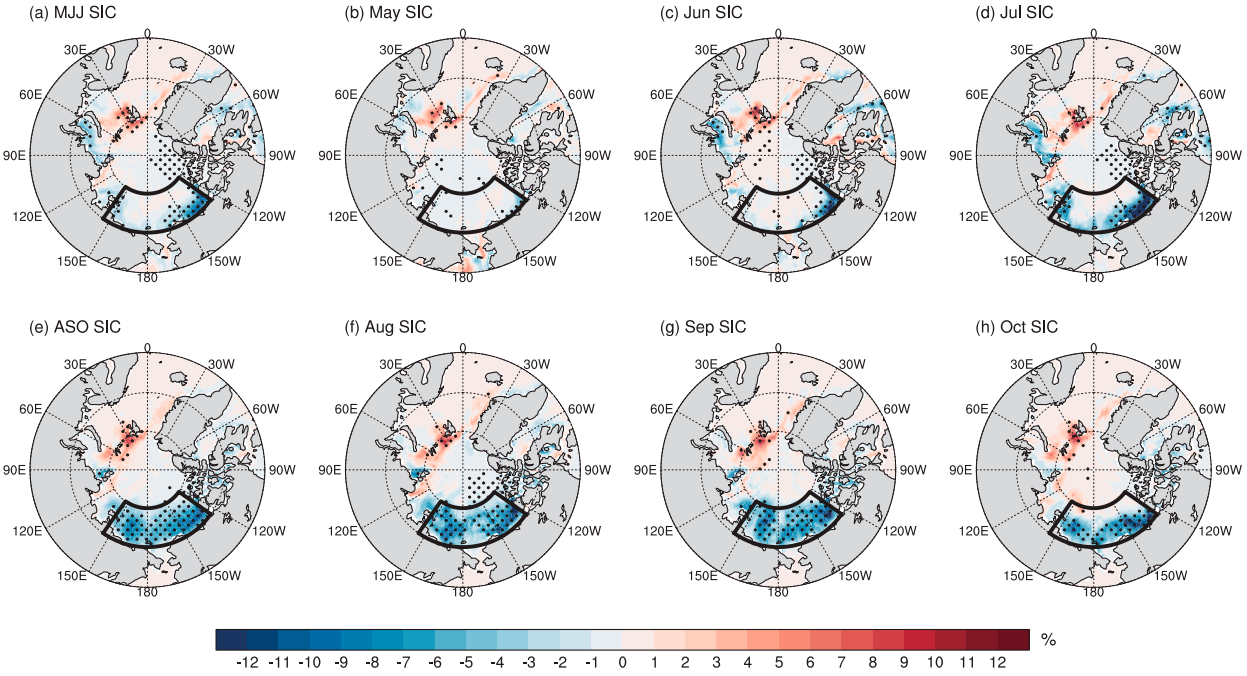


FIG. 7. Regressed SIC anomalies (shading; %) upon the normalized MJJ NAO index in (a) MJJ, (b) May, (c) June, (d) July, (e) ASO, (f) August, (g) September, and (h) October. Stippling represents SIC values above the 95% confidence level. The black box indicates the EsCB region. The regression coefficients were multiplied by a factor of −1.

(Fig. 4f), and a negative NAO-like circulation pattern begins to emerge. The negative NAO-like circulation anomalies are further intensified in June with its anticyclonic part covering most areas of the Arctic and its cyclonic part over the midlatitudinal North Atlantic (Fig. 4g). In July, the Arctic high pressure anomalies extend southward and separate the subtropical low pressure anomalies into two parts (Fig. 4h). Similar atmospheric patterns can also be observed in the upper level, suggesting an equivalent barotropic vertical structure (Figs. 4a–d). The preceding summer NAO-like circulation anomalies seem to be of importance for the EsCB SIC variability on the interannual time scale. We further display the correlation between the ASO EsCB sea ice and NAO indices in different preceding months (Fig. 5a). The boreal autumn EsCB sea ice is significantly correlated with the NAO index from the April–June to June–September seasons, with the maximum correlation being 0.6 in the May–July (MJJ) season (Fig. 5b). We also examine the relationship between the autumn EsCB sea ice and previous local atmospheric circulation anomalies like the Arctic dipole anomaly (Wu et al. 2012), and a moderately significant correlation can be detected (not shown).

We also perform composite analyses for high and low SIC years to illustrate the atmospheric circulation anomalies associated with the EsCB SIC variations (Fig. 6). Here, eight low (1968, 1977, 1990, 1993, 1998, 2003, 2007, 2012) and seven high (1994, 1996, 2001, 2006, 2009, 2013, 2018) SIC years are selected based on a threshold of 0.8 standard deviations of the EsCB index. Different thresholds (e.g., 0.6 and 0.7) are also used and the qualitative conclusion remains the same. In the MJJ season, the composite atmospheric circulation is approximately symmetric between high and low SIC years, manifested as a negative and positive NAO-like pattern for the low and high SIC years, respectively (Figs. 6a,c). In contrast, the atmospheric circulation anomalies are quite weak during the ASO season (Figs. 6b,d). The composite results again suggest that the previous rather than simultaneous atmospheric circulation anomalies are more likely to be responsible for the interannual variations of the EsCB sea ice.

4. Physical mechanisms for impacts of summer NAO on the following autumn EsCB SIC variations

Figure 7 shows the month-to-month evolution maps of SIC anomalies regressed upon the summer (MJJ) NAO index. Almost no significant SIC anomalies can be detected over the whole EsCB region in May (Fig. 7b). One month later, the SIC starts to reduce over the southeastern part of the Beaufort Sea in June, and the extent of these SIC anomalies gradually expands westward in the following months (Fig. 7). Around September, significant negative SIC anomalies almost cover the whole EsCB region. We next display the regression of the polar air temperature and wind anomalies onto the summer NAO index to investigate how the atmospheric anomalies affect the SIC over the EsCB region (Fig. 8). It is observed that the atmospheric circulation anomalies are much more prominent in the summer season than those in the autumn season (Figs. 8b,c). During the summer season (Fig. 8b), the negative NAO-like circulation is associated with a sandwich pattern of SAT anomalies with negative anomalies

Unauthenticated | Downloaded 11/13/26 12:37 PM UTC

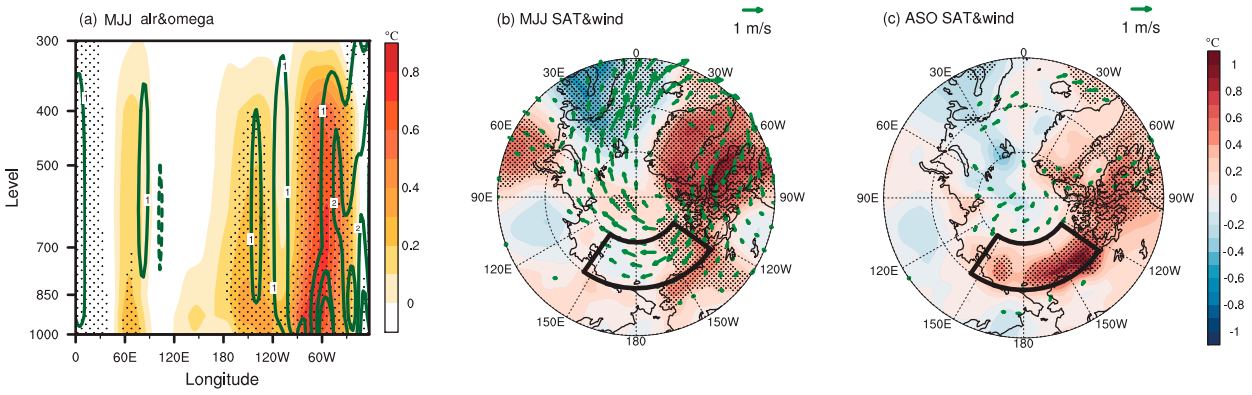


FIG. 8. (a) Meridional averaged (70°–80°N) air temperature (shading; °C) and vertical velocity anomalies (contours: solid lines are positive, dashed lines are negative; interval: 2×10^{-3} Pa s^{-1}) regressed onto the normalized MJJ NAO index. Only values exceeding the 95% confidence level are stippled (shading) or shown (contours). (b) Simultaneous surface air temperature (shading; °C) and surface wind anomalies (vectors; m s^{-1}) regressed onto the normalized MJJ NAO index. Only values exceeding the 95% confidence level are stippled (shading) or shown (vectors). (c) As in (b), but for ASO surface air temperature (shading; °C) and surface wind anomalies (vectors; m s^{-1}). The black box indicates the EsCB region. The regression coefficients were multiplied by a factor of −1.

over the western Barents Sea and positive anomalies around Greenland and the southern BK region. The NAO-related circumpolar anticyclonic anomalies tend to transport the warm air from Greenland toward the Beaufort Sea. The anomalous surface wind and SAT around Greenland are possibly due to the anomalous adiabatic subsidence motion locally (Fig. 8a). It is noted that the surface warming over the eastern EsCB part is also partially contributed by the effect of the local adiabatic heating associated with the anomalous subsidence despite that its amplitude is much weaker compared to that around Greenland. Since the EsCB region is generally covered by 1–2 years of thin ice (Babb et al. 2022), local positive SAT anomalies can easily trigger ice melting and lead to negative SIC anomalies. Compared with MJJ, the center of the warm anomalies near Greenland gradually weakens in autumn and moves westward to the EsCB region (Fig. 8c), indicating that the MJJ NAO-like atmospheric circulation anomalies still has a significant warming effect on the subsequent autumn EsCB area.

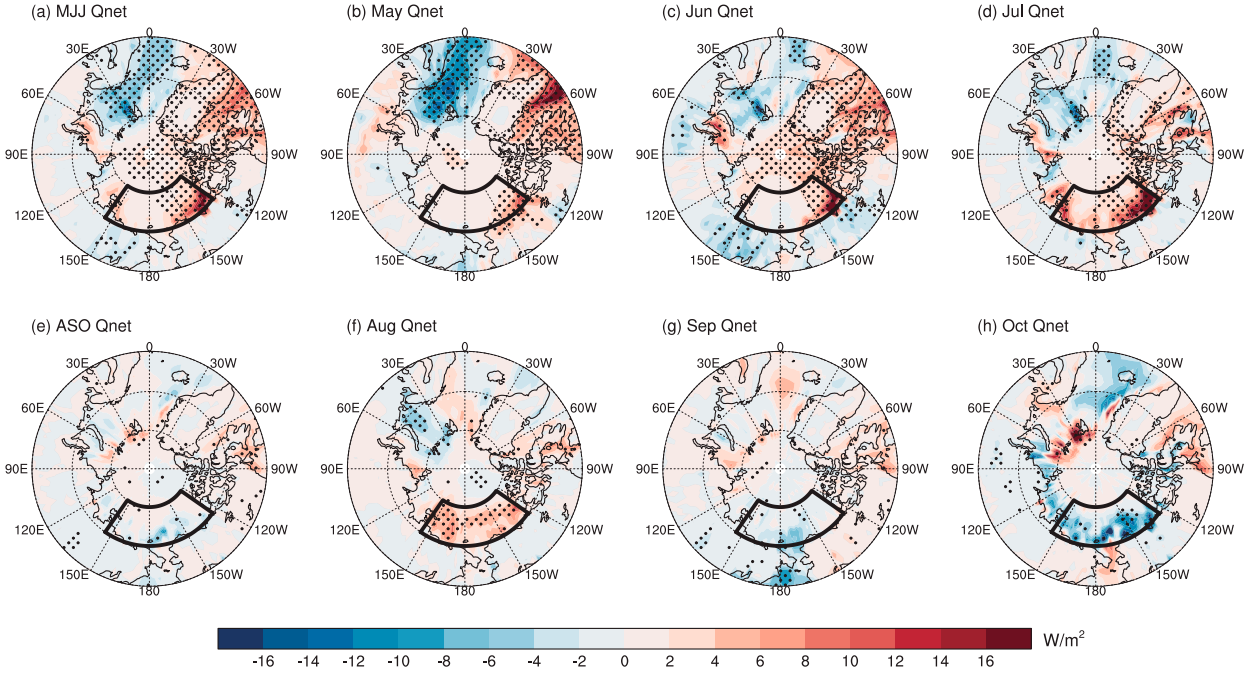


FIG. 9. Regressed net surface heat flux anomalies (shading; W m^{-2}) upon normalized MJJ NAO index in (a) MJJ, (b) May, (c) June, (d) July, (e) ASO, (f) August, (g) September, and (h) October. Positive direction is the downward radiation. Stippling represents values above the 95% confidence level. The black box indicates the EsCB region. The regression coefficients were multiplied by a factor of −1.

Unauthenticated | Downloaded 11/13/26 12:37 PM UTC

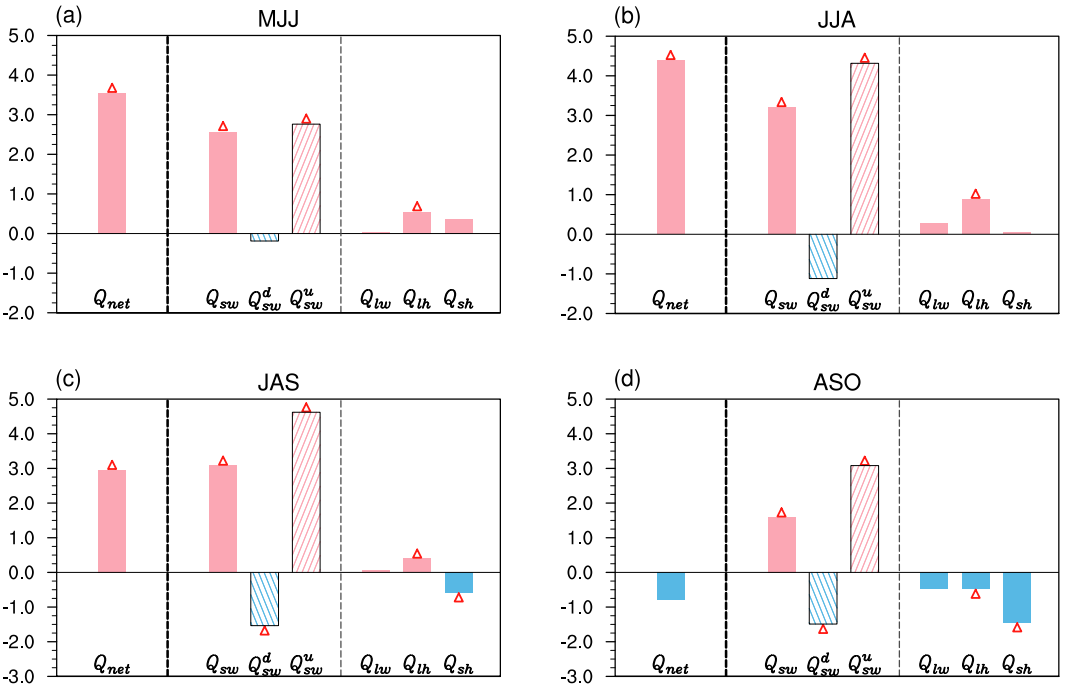


FIG. 10. Regression of each component of the net surface heat flux averaged in the EsCB area (W m^{-2}) upon the normalized MJJ NAO index in (a) MJJ, (b) JJA, (c) JAS, and (d) ASO. Positive direction is the downward radiation. Triangles indicate values above the 95% confidence level. The terms include the net surface heat flux (Q_{net}), net shortwave radiation (Q_{sw}), downward shortwave radiation (Q^d_{sw}), upward shortwave radiation (Q^u_{sw}), net longwave radiation (Q_{lw}), latent heat flux (Q_{lh}), and the sensible heat flux (Q_{sh}), respectively. The regression coefficients were multiplied by a factor of −1.

Previous studies argued that the atmospheric circulation can control the surface heat balance of Arctic sea ice growth and melting through energy exchange (Ding et al. 2017; Lee et al. 2011; Lee 2012; Baxter et al. 2019; Li et al. 2019; Luo et al. 2019). In addition to the direct effect of air temperature advection, the Arctic atmospheric circulation variations also have impacts on the sea ice by modifying the local net surface heat flux (Fig. 9). As shown in Fig. 9b, positive net surface heat flux anomalies appear over the Greenland–Beaufort Sea region in May during a negative NAO phase. Here, positive downward flux anomalies are defined as those into the ocean surface. The positive heat flux anomalies slowly extend westward to the EsCB region and lead to the stronger-than-normal melting of local sea ice (Figs. 9c,d). In August, the entire EsCB region is covered by the positive surface heat flux (Fig. 9f), and then net surface heat flux anomalies of the EsCB region change the sign after September (Figs. 9g,h). From May to August, the positive net heat flux anomalies heat the ocean surface over the EsCB region during the negative NAO phase, which leads to the reduction of the local SIC. In the following autumn, the negative heat flux anomalies suggest that the loss of the EsCB sea ice is largely responsible for the atmospheric anomalies rather than vice versa.

The net surface heat flux (Q_{net}) are further decomposed into the net shortwave radiation (Q_{sw}), net longwave radiation (Q_{lw}), latent heat flux (Q_{lh}), and sensible heat flux (Q_{sh}) to assess their respective contributions (Fig. 10). From the MJJ to JAS season, the EsCB net surface heat flux anomalies are all positive and dominated by the net shortwave radiation, favoring the local surface warming and SIC reduction (Figs. 10a–c). A further decomposition of the net shortwave radiation shows that its upward component (Q^u_{sw}) is the major contributor in these seasons, which can be enhanced by the sea ice–albedo positive feedback (Figs. 10a–c). In other words, from MJJ to JAS, the melted EsCB sea ice reduces the surface albedo. The increase in the net shortwave radiation, which is mainly contributed by the decrease in the upward shortwave radiation, leads to an amplification of the initial sea ice reduction. In ASO, the anomalous net surface heat flux reverses its sign, which is mainly contributed by the strongly enhanced negative sensible heat flux anomalies since JAS (Figs. 10c,d). Besides, the anomalous latent heat flux is positive from MJJ to JAS and negative during ASO, which also makes some contribution to the anomalous net surface heat flux (Fig. 10). The anomalous turbulent heat flux (i.e., latent and sensible heat fluxes) can warm the ocean surface and cause the reduction of the EsCB sea ice during summer. In subsequent autumn, the EsCB ocean becomes a heat source to the atmosphere via reverse signed turbulent heat flux anomalies.

The above analyses show that the preceding summer negative NAO-related atmospheric anomalies favor a reduction of

Unauthenticated | Downloaded 11/13/26 12:37 PM UTC

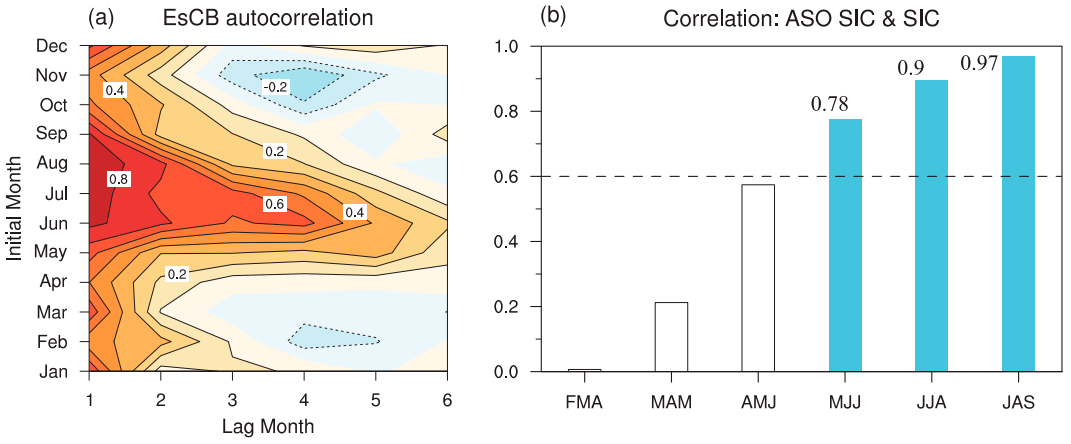


FIG. 11. (a) Autocorrelation of EsCB sea ice as a function of starting month. (b) Correlation coefficients between the ASO EsCB index and EsCB indices in previous seasons (bar). The dashed line represents the 95% confidence level.

the EsCB sea ice. We next demonstrate that the preceding NAO-related atmospheric signals can be preserved in the EsCB SIC anomalies several months later via the persistence of Arctic SIC (Deser et al. 2000; Bathiany et al. 2016), providing a potential way to understand the lagged relationship between the summer atmosphere and the subsequent autumn EsCB SIC. Figure 11 displays the EsCB SIC autocorrelation as a function of the starting month to exhibit the seasonality of its memory. It is evident that the EsCB SIC persistence exhibits a strong seasonal-dependent feature. The EsCB SIC signal during the boreal summer season can persist for up to 5–6 months, while the SIC persistence is largely limited to 1–2 months in other seasons (Fig. 11a). In particular, the correlation between the ASO and preceding MJJ EsCB SIC reaches as high as ~0.8 (Fig. 11b), suggesting that the reduction of MJJ sea ice in response to a negative NAO-like atmospheric condition can persist into the ASO season and be further amplified by the local positive feedbacks. In summary, the anomalous melting of EsCB sea ice in early summer can trigger a local positive feedback process that results in low values during the following autumn, and the MJJ NAO-like atmospheric circulation anomalies plays a crucial role in initiating this series of processes.

The observed linkage between the summer NAO-like circulation and the following autumn EsCB sea ice is further examined in historical simulations of the E3SM-1-0 model (see section 2), which is used here since it can realistically reproduce the observed climatology and interannual variability of the autumn EsCB sea ice (Fig. 12). Consistent with the observation, the simulated negative autumn EsCB SIC anomalies are closely associated with the positive geopotential high anomalies over the central Arctic and positive anomalies in

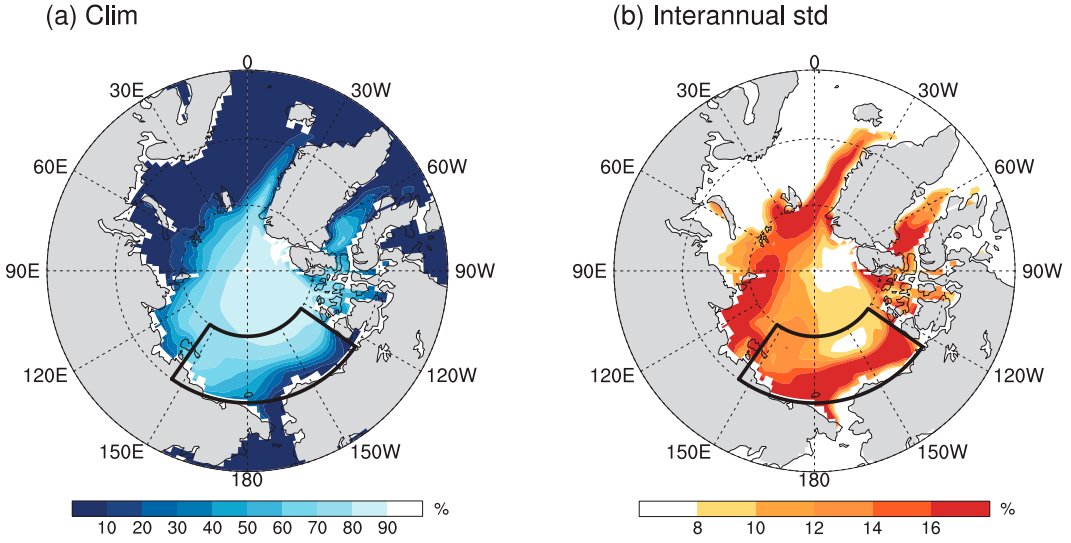


FIG. 12. Spatial distributions of autumn SIC (a) climatological mean (shading; %) and (b) the interannual standard deviation (shading; %) in the E3SM-1-0 model. The black box indicates the EsCB region.

Unauthenticated | Downloaded 11/13/26 12:37 PM UTC

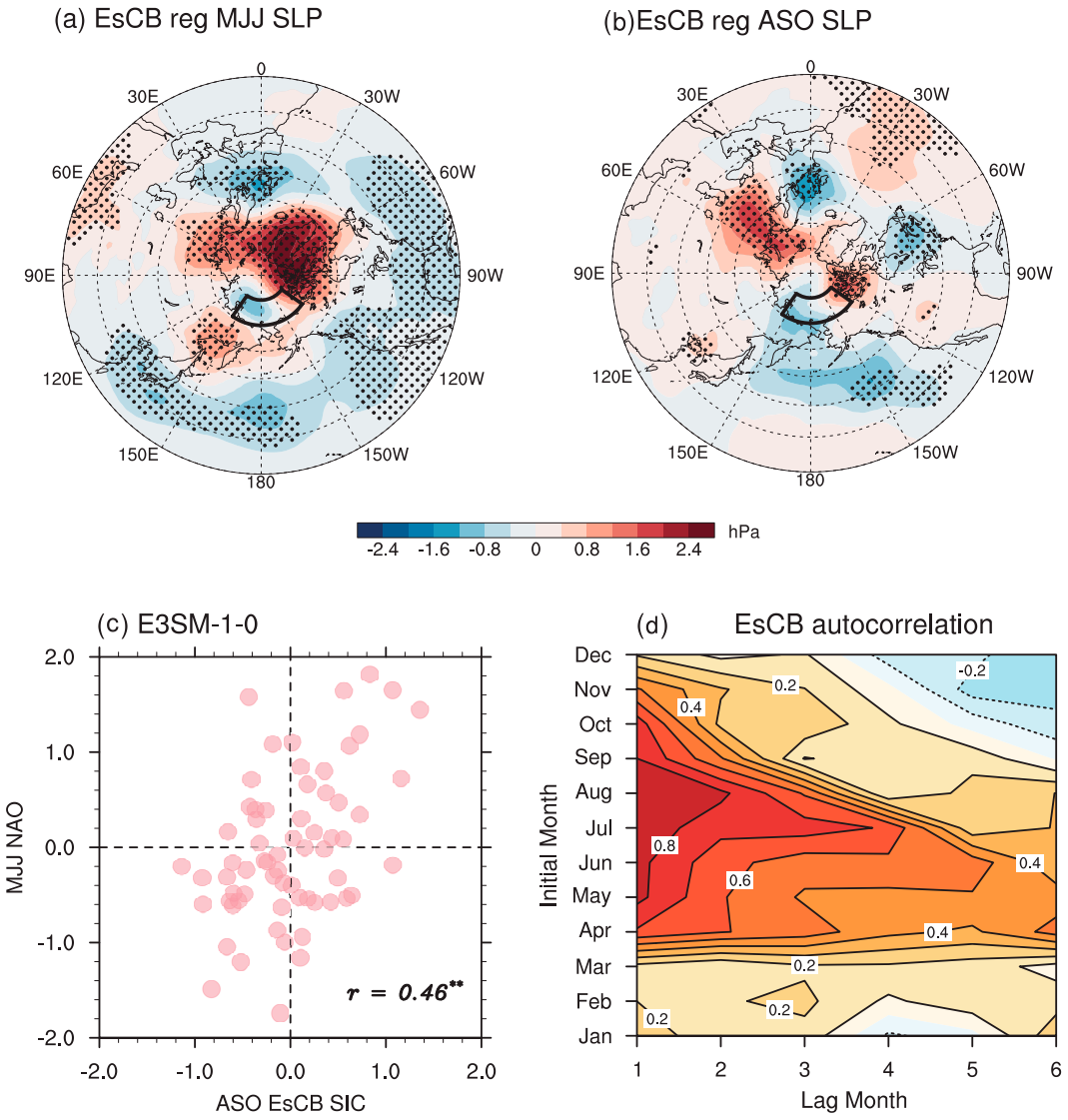


FIG. 13. Regressions of (a) MJJ, (b) ASO SLP (shading; hPa) anomalies upon the normalized EsCB index in the E3SM-1-0 model. (c) Scatterplot of the normalized MJJ NAO index and the EsCB index in the E3SM-1-0 model. The correlation coefficient (r) is labeled in the bottom-right corner. (d) Autocorrelation of EsCB sea ice as a function of starting month in the E3SM-1-0 model. Positive values are shown in solid lines, negative values in dashed lines, and 0 values are not displayed. In (a) and (b) only values exceeding the 95% confidence level are stippled (shading) or shown (vectors). The black box indicates the EsCB region. The regression coefficients were multiplied by a factor of −1.

the south in early summer, resembling a negative NAO-like atmospheric circulation despite a westward displacement of the southern center (Fig. 13a). The close linkage between the autumn EsCB sea ice and preceding summer NAO is further evidenced by their linear relationship (r = 0.46, statistically significant at the 95% confidence level) (Fig. 13c). In contrast, the simultaneous atmospheric circulation anomalies are relatively weak in association with the autumn EsCB sea ice (Fig. 13b). In addition, the well-reproduced strong persistence of EsCB sea ice during the boreal summer season (Fig. 13d) acts to retain the summer SIC anomalies into autumn. We further decompose the net surface heat flux in the E3SM-1-0 model (Fig. 14). From the MJJ to JAS season, the EsCB net surface heat flux anomalies are all positive, and the main contribution is from the net shortwave radiation (Figs. 14a–c). In ASO, the anomalous net surface heat flux reverses its sign (Fig. 14d), indicating that the loss of the autumn EsCB sea ice is largely responsible for the atmospheric anomalies. The reasonable consistency between the observation and model simulations increases confidence in explaining the physical relationship between the MJJ NAO-like atmospheric circulation anomaly and subsequent autumn EsCB sea ice on an interannual time scale.

Unauthenticated | Downloaded 11/13/26 12:37 PM UTC

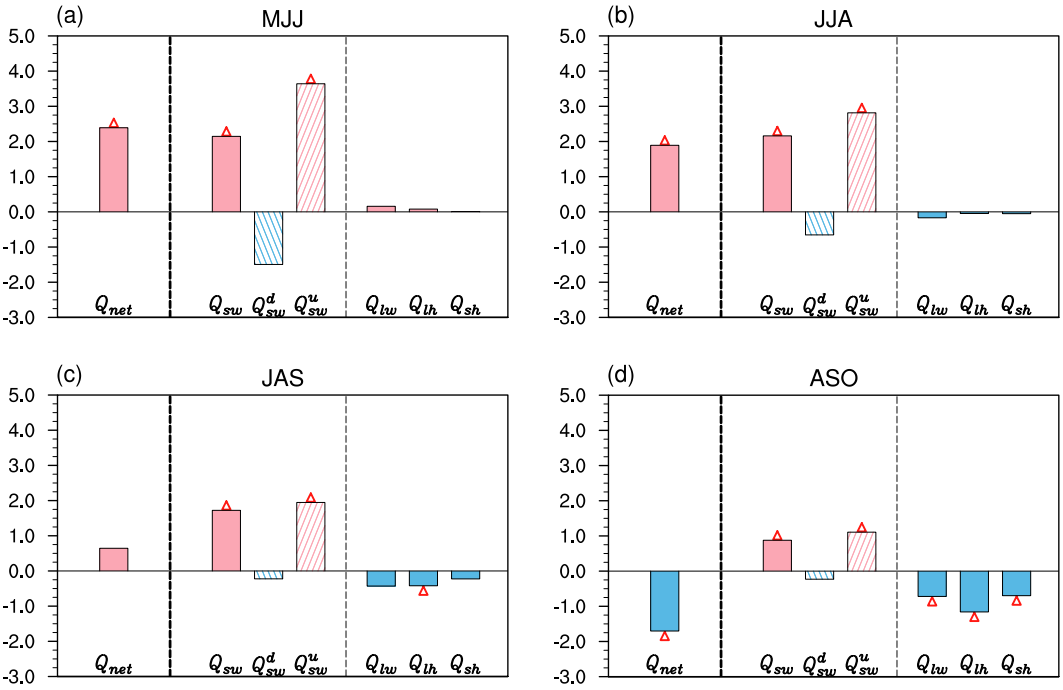


FIG. 14. Regression of each component of the net surface heat flux averaged in the (a) MJJ, (b) JJA, (c) JAS, and (d) ASO EsCB area (W m^{-2}) upon the normalized MJJ NAO index in the E3SM-1-0 model. Positive direction is the downward radiation. Triangles indicate values above the 95% confidence level. The terms include the net surface heat flux (Q_{net}), net shortwave radiation (Q_{sw}), downward shortwave radiation (Q^d_{sw}), upward shortwave radiation (Q^u_{sw}), net longwave radiation (Q_{lw}), latent heat flux (Q_{lh}), and the sensible heat flux (Q_{sh}), respectively. The regression coefficients were multiplied by a factor of −1.

5. Conclusions and discussion

The autumn EsCB sea ice variability has been receiving much attention in recent years due to its prominent climate impacts over Eurasia and North America (e.g., Kug et al. 2015; Chen and Wu 2018; Ding et al. 2021). So far, the physical causes of the interannual variability in the autumn EsCB sea ice are still poorly understood. In this study, we demonstrate that the year-to-year variations of the autumn EsCB sea ice are closely linked with the preceding summer NAO-like atmospheric circulation anomalies. An anomalous circumpolar anticyclone in association with the negative NAO-like phase favors warm SAT anomalies around Greenland due to the adiabatic subsidence motion during summer. The warm SAT anomalies can be transported toward the EsCB region via the anomalous easterlies. The warm advection together with the local positive sea ice–albedo feedback leads to the rapid melting of EsCB sea ice. Considering the long memory of the EsCB sea ice in summer, the SIC anomalies can persist into the subsequent autumn. Similar mechanisms operate in the positive NAO-like phase. The lagged relationship between the preceding summer atmospheric circulation and autumn EsCB sea ice can be realistically reproduced in the historical simulations of the E3SM-1-0 model.

The seasonal prediction of NAO has long been one of the most challenging scientific issues due to the high noise disturbance in the middle and high latitudes, especially in summer when its variability is relatively weak (Feldstein 2007; Hanna et al. 2015). The majority of previous works focused on the winter NAO variability and its possible physical linkages (Magnusdottir et al. 2004; Deser et al. 2004; Oshika et al. 2015; Gao et al. 2015), since the winter NAO is dynamically active. However, relatively limited attention is paid to the summer NAO variability and its possible physical drivers remain to be further investigated compared with the winter season (Folland et al. 2009; Osborne et al. 2020). Previous studies have demonstrated the effect of tropical SST on NAO based on observational analyses and numerical experiments (e.g., Czaja and Marshall 2001; Czaja and Frankignoul 2002; Peng et al. 2003; Gastineau and Frankignoul 2015; Chen et al. 2020). Here in Fig. 15 we show the spatial distribution of the correlation between the MJJ NAO index and the previous and simultaneous SST anomalies. The NAO-like atmospheric circulation anomalies are preceded by obvious tripole-like SST anomalies in the North Atlantic from the previous spring to concurrent early summer. The active interactive process between the local atmosphere and ocean favors the maintenance of NAO-like circulation anomalies. Although the exact predictability source of NAO in summer cannot be determined yet, our study shows that the occurrence of negative NAO-like patterns in summer can act as a potential precursor for the autumn EsCB sea ice variability.

Unauthenticated | Downloaded 11/13/26 12:37 PM UTC

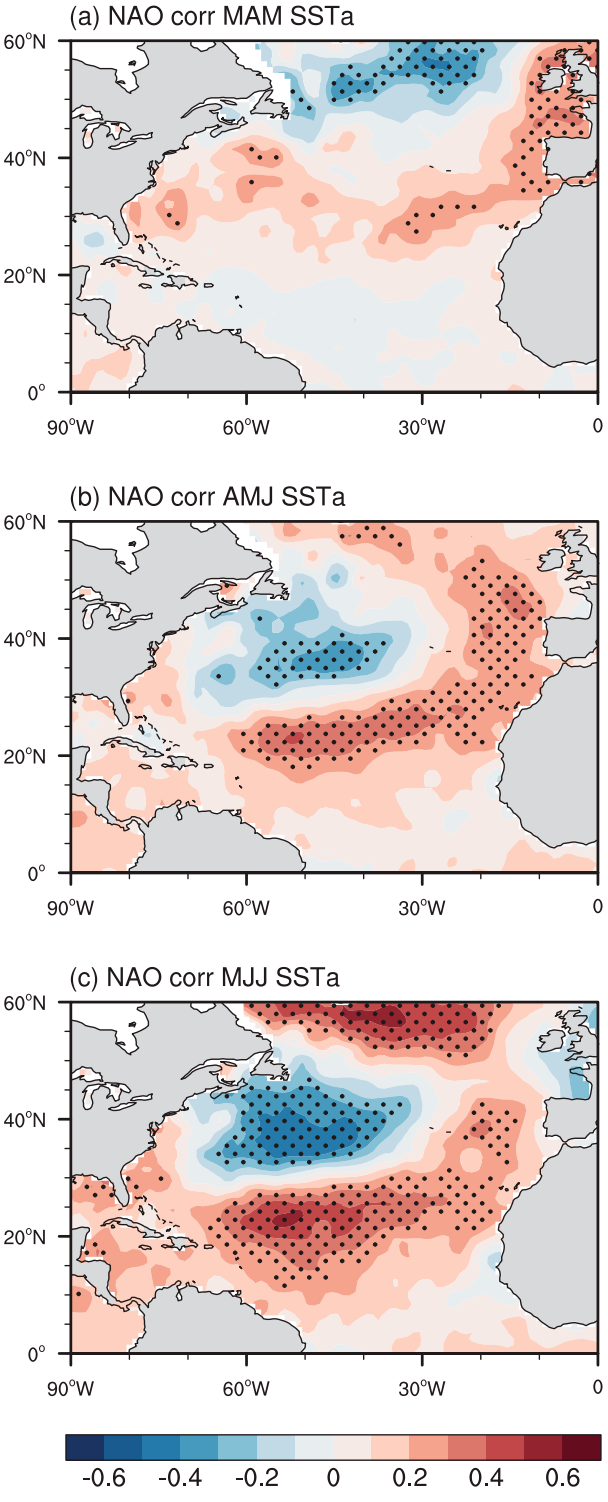


FIG. 15. Spatial distribution of correlation coefficient between the SST anomalies in (a) MAM, (b) AMJ, (c) MJJ and the MJJ NAO index. Only values exceeding the 95% confidence level are stippled.

Acknowledgments. This work was supported by the National Nature Science Foundation of China (42125501).

Data availability statement. The data supporting the findings of this study are available from the following resources: https://www.metoffice.gov.uk/hadobs/hadisst/data/download.html, https://psl.noaa.gov/data/gridded/data.ncep.reanalysis.html, https://www.cpc.ncep.noaa.gov/products/precip/CWlink/pna/nao.shtml, and https://esgf-node.llnl.gov/search/cmip6/.

REFERENCES

Aagaard, K., and E. C. Carmack, 1989: The role of sea ice and other fresh water in the Arctic circulation. *J. Geophys. Res.*, **94**, 14 485–14 498, https://doi.org/10.1029/JC094iC10p14485.

Babb, D. G., R. J. Galley, S. E. L. Howell, J. C. Landy, J. C. Stroeve, and D. G. Barber, 2022: Increasing multiyear sea ice loss in the Beaufort Sea: A new export pathway for the diminishing multiyear ice cover of the Arctic Ocean. *Geophys. Res. Lett.*, **49**, e2021GL097595, https://doi.org/10.1029/2021GL097595.

Barnston, A. G., and R. E. Livezey, 1987: Classification, seasonality and persistence of low-frequency atmospheric circulation patterns. *Mon. Wea. Rev.*, **115**, 1083–1126, https://doi.org/10.1175/1520-0493(1987)115<1083:CSAPOL>2.0.CO;2.

Barry, R. G., M. C. Serreze, J. A. Maslanik, and R. H. Preller, 1993: The Arctic sea ice-climate system: Observations and modeling. *Rev. Geophys.*, **31**, 397–422, https://doi.org/10.1029/93RG01998.

Bathiany, S., B. van der Bolt, M. S. Williamson, T. M. Lenton, M. Scheffer, E. H. van Nes, and D. Notz, 2016: Statistical indicators of Arctic sea-ice stability—Prospects and limitations. *Cryosphere*, **10**, 1631–1645, https://doi.org/10.5194/tc-10-1631-2016.

Baxter, I., and Coauthors, 2019: How tropical Pacific surface cooling contributed to accelerated sea ice melt from 2007 to 2012 as ice is thinned by anthropogenic forcing. *J. Climate*, **32**, 8583–8602, https://doi.org/10.1175/JCLI-D-18-0783.1.

Bliss, A. C., M. Steele, G. Peng, W. N. Meier, and S. Dickinson, 2019: Regional variability of Arctic sea ice seasonal change climate indicators from a passive microwave climate data record. *Environ. Res. Lett.*, **14**, 045003, https://doi.org/10.1088/1748-9326/aafb84.

Bogenschutz, P. A., S. Tang, P. M. Caldwell, S. Xie, W. Lin, and Y.-S. Chen, 2020: The E3SM version 1 single-column model. *Geosci. Model Dev.*, **13**, 4443–4458, https://doi.org/10.5194/gmd-13-4443-2020.

Budikova, D., 2009: Role of Arctic sea ice in global atmospheric circulation: A review. *Global Planet. Change*, **68**, 149–163, https://doi.org/10.1016/j.gloplacha.2009.04.001.

Carmack, E., and Coauthors, 2015: Toward quantifying the increasing role of oceanic heat in sea ice loss in the new Arctic. *Bull. Amer. Meteor. Soc.*, **96**, 2079–2105, https://doi.org/10.1175/BAMS-D-13-00177.1.

Cavalieri, D. J., and C. L. Parkinson, 2012: Arctic sea ice variability and trends, 1979–2010. *Cryosphere*, **6**, 881–889, https://doi.org/10.5194/tc-6-881-2012.

Chen, S., and R. Wu, 2018: Impacts of early autumn Arctic sea ice concentration on subsequent spring Eurasian surface air temperature variations. *Climate Dyn.*, **51**, 2523–2542, https://doi.org/10.1007/s00382-017-4026-x.

Unauthenticated | Downloaded 11/13/26 12:37 PM UTC

——, ——, and W. Chen, 2020: Strengthened connection between springtime North Atlantic Oscillation and North Atlantic tripole SST pattern since the late 1980s. *J. Climate*, **33**, 2007–2022, https://doi.org/10.1175/JCLI-D-19-0628.1.

Chen, Z., R. Wu, and W. Chen, 2014: Impacts of autumn Arctic sea ice concentration changes on the East Asian winter monsoon variability. *J. Climate*, **27**, 5433–5450, https://doi.org/10.1175/JCLI-D-13-00731.1.

Close, S., M.-N. Houssais, and C. Herbaut, 2015: Regional dependence in the timing of onset of rapid decline in Arctic sea ice concentration. *J. Geophys. Res. Oceans*, **120**, 8077–8098, https://doi.org/10.1002/2015JC011187.

Comiso, J. C., 2002: A rapidly declining perennial sea ice cover in the Arctic. *Geophys. Res. Lett.*, **29**, 1956, https://doi.org/10.1029/2002GL015650.

——, C. L. Parkinson, R. Gersten, and L. Stock, 2008: Accelerated decline in the Arctic sea ice cover. *Geophys. Res. Lett.*, **35**, L01703, https://doi.org/10.1029/2007GL031972.

Cui, H., F. Qiao, Q. Shu, Y. Song, and C. Jiang, 2015: Causes for different spatial distributions of minimum Arctic sea-ice extent in 2007 and 2012. *Acta Oceanol. Sin.*, **34**, 94–101, https://doi.org/10.1007/s13131-015-0676-x.

Curry, J. A., J. L. Schramm, and E. E. Ebert, 1995: Sea ice-albedo climate feedback mechanism. *J. Climate*, **8**, 240–247, https://doi.org/10.1175/1520-0442(1995)008<0240:SIACFM>2.0.CO;2.

Czaja, A., and J. Marshall, 2001: Observations of atmosphere-ocean coupling in the North Atlantic. *Quart. J. Roy. Meteor. Soc.*, **127**, 1893–1916, https://doi.org/10.1002/qj.49712757603.

——, and C. Frankignoul, 2002: Observed impact of Atlantic SST anomalies on the North Atlantic Oscillation. *J. Climate*, **15**, 606–623, https://doi.org/10.1175/1520-0442(2002)015<0606:OIOASA>2.0.CO;2.

Deser, C., J. E. Walsh, and M. S. Timlin, 2000: Arctic sea ice variability in the context of recent atmospheric circulation trends. *J. Climate*, **13**, 617–633, https://doi.org/10.1175/1520-0442(2000)013<0617:ASIVIT>2.0.CO;2.

——, G. Magnusdottir, R. Saravanan, and A. Phillips, 2004: The effects of North Atlantic SST and sea ice anomalies on the winter circulation in CCM3. Part II: Direct and indirect components of the response. *J. Climate*, **17**, 877–889, https://doi.org/10.1175/1520-0442(2004)017<0877:TEONAS>2.0.CO;2.

Ding, Q., and Coauthors, 2017: Influence of high-latitude atmospheric circulation changes on summertime Arctic sea ice. *Nat. Climate Change*, **7**, 289–295, https://doi.org/10.1038/nclimate3241.

Ding, S., B. Wu, and W. Chen, 2021: Dominant characteristics of early autumn Arctic sea ice variability and its impact on winter Eurasian climate. *J. Climate*, **34**, 1825–1846, https://doi.org/10.1175/JCLI-D-19-0834.1.

Eisenman, I., 2010: Geographic muting of changes in the Arctic sea ice cover. *Geophys. Res. Lett.*, **37**, L16501, https://doi.org/10.1029/2010GL043741.

Feldstein, S. B., 2007: The dynamics of the North Atlantic Oscillation during the summer season. *Quart. J. Roy. Meteor. Soc.*, **133**, 1509–1518, https://doi.org/10.1002/qj.107.

Folland, C. K., J. Knight, H. W. Linderholm, D. Fereday, S. Ineson, and J. W. Hurrell, 2009: The summer North Atlantic Oscillation: Past, present, and future. *J. Climate*, **22**, 1082–1103, https://doi.org/10.1175/2008JCLI2459.1.

Francis, J. A., W. Chan, D. J. Leathers, J. R. Miller, and D. E. Veron, 2009: Winter Northern Hemisphere weather patterns remember summer Arctic sea-ice extent. *Geophys. Res. Lett.*, **36**, L07503, https://doi.org/10.1029/2009GL037274.

Gao, Y., and Coauthors, 2015: Arctic sea ice and Eurasian climate: A review. *Adv. Atmos. Sci.*, **32**, 92–114, https://doi.org/10.1007/s00376-014-0009-6.

Gastineau, G., and C. Frankignoul, 2015: Influence of the North Atlantic SST variability on the atmospheric circulation during the twentieth century. *J. Climate*, **28**, 1396–1416, https://doi.org/10.1175/JCLI-D-14-00424.1.

Gillett, N. P., D. A. Stone, P. A. Stott, T. Nozawa, A. Y. Karpechko, G. C. Hegerl, M. F. Wehner, and P. D. Jones, 2008: Attribution of polar warming to human influence. *Nat. Geosci.*, **1**, 750–754, https://doi.org/10.1038/ngeo338.

Golaz, J.-C., and Coauthors, 2019: The DOE E3SM coupled model version 1: Overview and evaluation at standard resolution. *J. Adv. Model. Earth Syst.*, **11**, 2089–2129, https://doi.org/10.1029/2018MS001603.

Hanna, E., T. E. Cropper, P. D. Jones, A. A. Scaife, and R. Allan, 2015: Recent seasonal asymmetric changes in the NAO (a marked summer decline and increased winter variability) and associated changes in the AO and Greenland blocking index. *Int. J. Climatol.*, **35**, 2540–2554, https://doi.org/10.1002/joc.4157.

Herbaut, C., M.-N. Houssais, S. Close, and A.-C. Blaizot, 2015: Two wind-driven modes of winter sea ice variability in the Barents Sea. *Deep-Sea Res. I*, **106**, 97–115, https://doi.org/10.1016/j.dsr.2015.10.005.

Honda, M., J. Inoue, and S. Yamane, 2009: Influence of low Arctic sea-ice minima on anomalously cold Eurasian winters. *Geophys. Res. Lett.*, **36**, L08707, https://doi.org/10.1029/2008GL037079.

Hu, C., S. Yang, Q. Wu, Z. Li, J. Chen, K. Deng, T. Zhang, and C. Zhang, 2016: Shifting El Niño inhibits summer Arctic warming and Arctic sea-ice melting over the Canada Basin. *Nat. Commun.*, **7**, 11721, https://doi.org/10.1038/ncomms11721.

Hurrell, J. W., 1995: Decadal trends in the North Atlantic Oscillation: Regional temperatures and precipitation. *Science*, **269**, 676–679, https://doi.org/10.1126/science.269.5224.676.

Jeong, H., and Coauthors, 2020: Impacts of ice-shelf melting on water-mass transformation in the Southern Ocean from E3SM simulations. *J. Climate*, **33**, 5787–5807, https://doi.org/10.1175/JCLI-D-19-0683.1.

Kalnay, E., and Coauthors, 1996: The NCEP/NCAR 40-Year Reanalysis Project. *Bull. Amer. Meteor. Soc.*, **77**, 437–472, https://doi.org/10.1175/1520-0477(1996)077<0437:TNYRP>2.0.CO;2.

Kirchmeier-Young, M. C., F. W. Zwiers, and N. P. Gillett, 2017: Attribution of extreme events in Arctic sea ice extent. *J. Climate*, **30**, 553–571, https://doi.org/10.1175/JCLI-D-16-0412.1.

Kug, J.-S., J.-H. Jeong, Y.-S. Jang, B.-M. Kim, C. K. Folland, S.-K. Min, and S.-W. Son, 2015: Two distinct influences of Arctic warming on cold winters over North America and East Asia. *Nat. Geosci.*, **8**, 759–762, https://doi.org/10.1038/ngeo2517.

Kwok, R., and D. A. Rothrock, 2009: Decline in Arctic sea ice thickness from submarine and ICESat records: 1958–2008. *Geophys. Res. Lett.*, **36**, L15501, https://doi.org/10.1029/2009GL039035.

Lee, D. Y., W. Lin, and M. R. Petersen, 2020: Wintertime Arctic Oscillation and North Atlantic Oscillation and their impacts on the Northern Hemisphere climate in E3SM. *Climate Dyn.*, **55**, 1105–1124, https://doi.org/10.1007/s00382-020-05316-0.

Lee, S., 2012: Testing of the tropically excited Arctic warming mechanism (TEAM) with traditional El Niño and La Niña. *J. Climate*, **25**, 4015–4022, https://doi.org/10.1175/JCLI-D-12-00055.1.

Unauthenticated | Downloaded 11/13/26 12:37 PM UTC

——, T. Gong, N. Johnson, S. B. Feldstein, and D. Pollard, 2011: On the possible link between tropical convection and the Northern Hemisphere Arctic surface air temperature change between 1958 and 2001. *J. Climate*, **24**, 4350–4367, https://doi.org/10.1175/2011JCLI4003.1.

Lei, R., X. Tian-Kunze, M. Leppäranta, J. Wang, L. Kaleschke, and Z. Zhang, 2016: Changes in summer sea ice, albedo, and portioning of surface solar radiation in the Pacific sector of Arctic Ocean during 1982–2009. *J. Geophys. Res. Oceans*, **121**, 5470–5486, https://doi.org/10.1002/2016JC011831.

Li, J. P., and J. X. L. Wang, 2003: A new North Atlantic Oscillation index and its variability. *Adv. Atmos. Sci.*, **20**, 661–676, https://doi.org/10.1007/BF02915394.

Li, Z., W. Zhang, M. F. Stuecker, H. Xu, F.-F. Jin, and C. Liu, 2019: Different effects of two ENSO types on Arctic surface temperature in boreal winter. *J. Climate*, **32**, 4943–4961, https://doi.org/10.1175/JCLI-D-18-0761.1.

Lind, S., R. B. Ingvaldsen, and T. Furevik, 2018: Arctic warming hotspot in the northern Barents Sea linked to declining sea-ice import. *Nat. Climate Change*, **8**, 634–639, https://doi.org/10.1038/s41558-018-0205-y.

Liu, L., W. Zhang, and C. Liu, 2023: Multidecadal variability of sea ice in the East Siberia–Beaufort Sea region and its linkage with the Atlantic multidecadal oscillation. *Acta Meteor. Sin.*, **81**, 137–151, https://doi.org/10.11676/qxxb2023.20220080.

Liu, Z., and Coauthors, 2021: Acceleration of western Arctic sea ice loss linked to the Pacific North American pattern. *Nat. Commun.*, **12**, 1519, https://doi.org/10.1038/s41467-021-21830-z.

Luo, R., Z. Wu, P. Zhang, and J. Dou, 2019: Potential influence of a developing La Niña on the sea-ice reduction in the Barents-Kara Seas. *Atmos.–Ocean*, **57**, 182–194, https://doi.org/10.1080/07055900.2019.1587375.

Magnusdottir, G., C. Deser, and R. Saravanan, 2004: The effects of North Atlantic SST and sea ice anomalies on the winter circulation in CCM3. Part I: Main features and storm track characteristics of the response. *J. Climate*, **17**, 857–876, https://doi.org/10.1175/1520-0442(2004)017<0857:TEONAS>2.0.CO;2.

Meier, W. N., J. Stroeve, and F. Fetterer, 2007: Whither Arctic sea ice? A clear signal of decline regionally, seasonally and extending beyond the satellite record. *Ann. Glaciol.*, **46**, 428–434, https://doi.org/10.3189/172756407782871170.

Mori, M., M. Watanabe, H. Shiogama, J. Inoue, and M. Kimoto, 2014: Robust Arctic sea-ice influence on the frequent Eurasian cold winters in past decades. *Nat. Geosci.*, **7**, 869–873, https://doi.org/10.1038/ngeo2277.

——, Y. Kosaka, M. Watanabe, H. Nakamura, and M. Kimoto, 2019: A reconciled estimate of the influence of Arctic sea-ice loss on recent Eurasian cooling. *Nat. Climate Change*, **9**, 123–129, https://doi.org/10.1038/s41558-018-0379-3.

Nie, Y., H.-L. Ren, Y. Zhang, and P. Zhang, 2022: Roles of atmospheric variability and Arctic sea ice in the asymmetric Arctic–Eurasia temperature connection on subseasonal time scale. *J. Climate*, **35**, 7575–7594, https://doi.org/10.1175/JCLI-D-21-0771.1.

Notz, D., and SIMIP Community, 2020: Arctic sea ice in CMIP6. *Geophys. Res. Lett.*, **47**, e2019GL086749, https://doi.org/10.1029/2019GL086749.

——, A. Jahn, M. M. Holland, E. C. Hunke, F. Massonnet, J. Stroeve, B. Tremblay, and M. Vancoppenolle, 2016: The CMIP6 Sea-Ice Model Intercomparison Project (SIMIP): Understanding sea ice through climate-model simulations. *Geosci. Model Dev.*, **9**, 3427–3446, https://doi.org/10.5194/gmd-9-3427-2016.

Nussbaumer, E. A., and R. T. Pinker, 2012: The role of shortwave radiation in the 2007 Arctic sea ice anomaly. *Geophys. Res. Lett.*, **39**, L15808, https://doi.org/10.1029/2012GL052415.

Ogi, M., and J. M. Wallace, 2007: Summer minimum Arctic sea ice extent and the associated summer atmospheric circulation. *Geophys. Res. Lett.*, **34**, L12705, https://doi.org/10.1029/2007GL029897.

Onarheim, I. H., T. Eldevik, L. H. Smedsrud, and J. C. Stroeve, 2018: Seasonal and regional manifestation of Arctic sea ice loss. *J. Climate*, **31**, 4917–4932, https://doi.org/10.1175/JCLI-D-17-0427.1.

Osborne, J. M., M. Collins, J. A. Screen, S. I. Thomson, and N. Dunstone, 2020: The North Atlantic as a driver of summer atmospheric circulation. *J. Climate*, **33**, 7335–7351, https://doi.org/10.1175/JCLI-D-19-0423.1.

Oshika, M., Y. Tachibana, and T. Nakamura, 2015: Impact of the winter North Atlantic Oscillation (NAO) on the Western Pacific (WP) pattern in the following winter through Arctic sea ice and ENSO: Part I—Observational evidence. *Climate Dyn.*, **45**, 1355–1366, https://doi.org/10.1007/s00382-014-2384-1.

Parkinson, C. L., 2014: Global sea ice coverage from satellite data: Annual cycle and 35-yr trends. *J. Climate*, **27**, 9377–9382, https://doi.org/10.1175/JCLI-D-14-00605.1.

——, and D. J. Cavalieri, 1989: Arctic sea ice 1973–1987: Seasonal, regional, and interannual variability. *J. Geophys. Res.*, **94**, 14 499–14 523, https://doi.org/10.1029/JC094iC10p14499.

Pavlova, O., V. Pavlov, and S. Gerland, 2014: The impact of winds and sea surface temperatures on the Barents Sea ice extent, a statistical approach. *J. Mar. Syst.*, **130**, 248–255, https://doi.org/10.1016/j.jmarsys.2013.02.011.

Peng, G., and W. N. Meier, 2017: Temporal and regional variability of Arctic sea-ice coverage from satellite data. *Ann. Glaciol.*, **59**, 191–200, https://doi.org/10.1017/aog.2017.32.

Peng, S., W. A. Robinson, and S. Li, 2003: Mechanisms for the NAO responses to the North Atlantic SST tripole. *J. Climate*, **16**, 1987–2004, https://doi.org/10.1175/1520-0442(2003)016<1987:MFTNRT>2.0.CO;2.

Petersen, M. R., and Coauthors, 2019: An evaluation of the ocean and sea ice climate of E3SM using MPAS and interannual CORE-II forcing. *J. Adv. Model. Earth Syst.*, **11**, 1438–1458, https://doi.org/10.1029/2018MS001373.

Petoukhov, V., and V. A. Semenov, 2010: A link between reduced Barents-Kara sea ice and cold winter extremes over northern continents. *J. Geophys. Res.*, **115**, D21111, https://doi.org/10.1029/2009JD013568.

Rayner, N. A., D. E. Parker, E. B. Horton, C. K. Folland, L. V. Alexander, D. P. Rowell, E. C. Kent, and A. Kaplan, 2003: Global analyses of sea surface temperature, sea ice, and night marine air temperature since the late nineteenth century. *J. Geophys. Res.*, **108**, 4407, https://doi.org/10.1029/2002JD002670.

Rothrock, D. A., Y. Yu, and G. A. Maykut, 1999: Thinning of the Arctic sea-ice cover. *Geophys. Res. Lett.*, **26**, 3469–3472, https://doi.org/10.1029/1999GL010863.

Schlichtholz, P., 2011: Influence of oceanic heat variability on sea ice anomalies in the Nordic seas. *Geophys. Res. Lett.*, **38**, L05705, https://doi.org/10.1029/2010GL045894.

Screen, J., C. Deser, I. Simmonds, and R. Tomas, 2014: Atmospheric impacts of Arctic sea-ice loss, 1979–2009: Separating forced change from atmospheric internal variability. *Climate Dyn.*, **43**, 333–344, https://doi.org/10.1007/s00382-013-1830-9.

Unauthenticated | Downloaded 11/13/26 12:37 PM UTC

Serreze, M. C., M. M. Holland, and J. Stroeve, 2007: Perspectives on the Arctic's shrinking sea-ice cover. *Science*, **315**, 1533–1536, https://doi.org/10.1126/science.1139426.

Spreen, G., R. Kwok, and D. Menemenlis, 2011: Trends in Arctic sea ice drift and role of wind forcing: 1992–2009. *Geophys. Res. Lett.*, **38**, L19501, https://doi.org/10.1029/2011GL048970.

Stroeve, J., and D. Notz, 2018: Changing state of Arctic sea ice across all seasons. *Environ. Res. Lett.*, **13**, 103001, https://doi.org/10.1088/1748-9326/aade56.

——, M. M. Holland, W. Meier, T. Scambos, and M. Serreze, 2007: Arctic sea ice decline: Faster than forecast. *Geophys. Res. Lett.*, **34**, L09501, https://doi.org/10.1029/2007GL029703.

——, M. Serreze, S. Drobot, S. Gearheard, M. Holland, J. Maslanik, W. Meier, and T. Scambos, 2008: Arctic sea ice extent plummets in 2007. *Eos, Trans. Amer. Geophys. Union*, **89**, 13–14, https://doi.org/10.1029/2008EO020001.

Ukita, J., M. Honda, H. Nakamura, Y. Tachibana, D. J. Cavalieri, C. L. Parkinson, H. Koide, and K. Yamamoto, 2016: Northern Hemisphere sea ice variability: Lag structure and its implications. *Tellus*, **59A**, 261–272, https://doi.org/10.1111/j.1600-0870.2006.00223.x.

Veneziani, M., and Coauthors, 2022: An evaluation of the E3SMv1 Arctic ocean and sea-ice regionally refined model. *Geosci. Model Dev.*, **15**, 3133–3160, https://doi.org/10.5194/gmd-15-3133-2022.

Vihma, T., 2014: Effects of Arctic sea ice decline on weather and climate: A review. *Surv. Geophys.*, **35**, 1175–1214, https://doi.org/10.1007/s10712-014-9284-0.

Wallace, J. M., and D. S. Gutzler, 1981: Teleconnections in the geopotential height field during the Northern Hemisphere winter. *Mon. Wea. Rev.*, **109**, 784–812, https://doi.org/10.1175/1520-0493(1981)109<0784:TITGHF>2.0.CO;2.

Wang, J., L. A. Mysak, and R. G. Ingram, 1994: Interannual variability of sea-ice cover in Hudson Bay, Baffin Bay and the Labrador Sea. *Atmos.–Ocean*, **32**, 421–447, https://doi.org/10.1080/07055900.1994.9649505.

——, J. Zhang, E. Watanabe, M. Ikeda, K. Mizobata, J. E. Walsh, X. Bai, and B. Wu, 2009: Is the dipole anomaly a major driver to record lows in Arctic summer sea ice extent? *Geophys. Res. Lett.*, **36**, L05706, https://doi.org/10.1029/2008GL036706.

Wu, B., and M. A. Johnson, 2007: A seesaw structure in SLP anomalies between the Beaufort Sea and the Barents Sea. *Geophys. Res. Lett.*, **34**, L05811, https://doi.org/10.1029/2006GL028333.

——, J. Wang, and J. E. Walsh, 2006: Dipole anomaly in the winter Arctic atmosphere and its association with sea ice motion. *J. Climate*, **19**, 210–225, https://doi.org/10.1175/JCLI3619.1.

——, J. Su, and R. Zhang, 2011: Effects of autumn-winter Arctic sea ice on winter Siberian high. *Chin. Sci. Bull.*, **56**, 3220–3228, https://doi.org/10.1007/s11434-011-4696-4.

——, J. E. Overland, and R. D'Arrigo, 2012: Anomalous Arctic surface wind patterns and their impacts on September sea ice minima and trend. *Tellus*, **64A**, 18590, https://doi.org/10.3402/tellusa.v64i0.18590.

Zhang, J., R. Lindsay, A. Schweiger, and M. Steele, 2013: The impact of an intense summer cyclone on 2012 Arctic sea ice retreat. *Geophys. Res. Lett.*, **40**, 720–726, https://doi.org/10.1002/grl.50190.

Zuo, J., H. Ren, B. Wu, and W. Li, 2016: Predictability of winter temperature in China from previous autumn Arctic sea ice. *Climate Dyn.*, **47**, 2331–2343, https://doi.org/10.1007/s00382-015-2966-6.

Unauthenticated | Downloaded 11/13/26 12:37 PM UTC